HIGH-TEMPERATURE PROCESSING OF SOLIDS IN PLANETARY EMBRYO BOW SHOCKS. **A. C. Boley** [1], **M. A. Morris**[2,3], and **S. J. Desch**[2]. [1]Department of Astronomy, University of Florida, Gainesville, FL 32611. [2]School of Earth and Space Exploration, Arizona State University, Tempe, AZ 85287. [3]Center for Meteorite Studies, Arizona State University, Tempe, AZ 85287. (aaron.boley@gmail.com) .

Introduction: Dynamical interactions between planetoids and planets are a natural consequence of planet formation and can place large bodies on eccentric and/or inclined orbits [1-3]. If gas is present during scattering events, as is suggested by recent models of Mars's low mass [3,4] and new age estimates for Mars's formation [5], a wide range of nebular shocks can be produced. Any solids that pass through these shocks could be altered significantly through rapid melting followed by crystallization during cooling [6-8]. Some of the resulting processed solids should be incorporated into meteoritic parent bodies, creating a record of the frequency and strengths of shocks that must have been present in the solar nebula. Chondrules are among the most well-studied of processed solids found in meteorites [9-14], and seem to have formed in nebular shocks [7,15,16].

In this study, we use three-dimensional radiation hydrodynamics with a proper equation of state to examine the thermal histories of solids as they pass through nebular bow shocks. This work is largely set apart from previous bow-shock studies for the following reasons: First, we build on the results of [17] and consider planetoids (radius $\sim$ 3000 km) instead of planetesimals [18]. Planetesimals have been shown to produce too rapid cooling rates [8] and are likely to accrete chondrules after melting due to the shock's small standoff distance [17]. Second, we directly integrate solids along with the hydrodynamics calculations, explicitly coupling solids and gas through drag. Following the trajectories of these solids allows us to measure self-consistent temperature and pressure histories as a function of impact parameter from the planetoid. Third, the simulations are run in 3D. Previous studies have used 2D calculations to reduce computational demands [e.g., 17], but we find that such simplifications result in a marked change in the shock structure. Fourth, we include a proper equation of state (EOS) that includes the rotational and vibrational modes of molecular hydrogen, as well as molecular hydrogen dissociation [19,20]. While other studies have included H_2 dissociation in 1D shocks, the effects of H_2 temperature buffering will alter 3D shock structures. For example, dissociation will produce cooler post-shock temperatures, higher post-shock densities, and smaller shock standoff distances due to absorption of heat by internal molecular processes. Fifth, radiative transfer is included (simulations in progress), where the opacity of the gas is tied directly to the spatial distribution of the integrated solids.

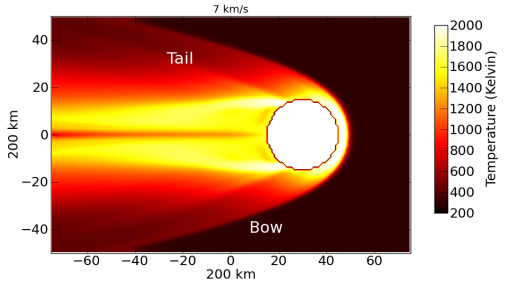

Figure 1: Cross section of a bow shock simulation with a 3000 km planetoid moving at 7 km s^{-1} with respect to the local gas. The simulation is run adiabatically, but with a proper equation of state that takes into account the thermal and dynamical effects of rotational and vibrational models of H_2, as well as H_2 dissociation. Particles are run along with the simulation to self-consistently capture the thermal profile. The bow and tail shocks are explicitly labeled.

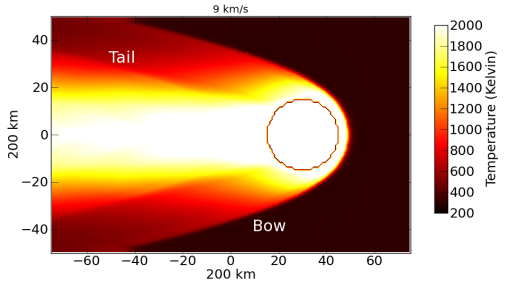

Figure 2: Similar to Figure 1, but the planetoid is moving at 9 km s^{-1} with respect to the local gas. Note the clear development of a bow and tail shock.

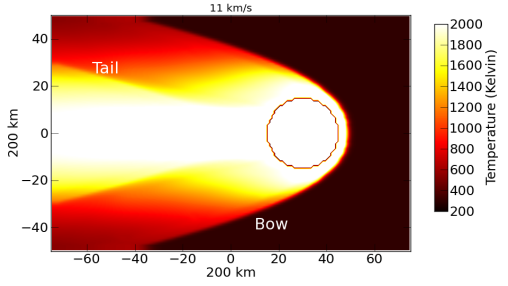

Figure 3: Similar to Figure 2, but the planetoid is moving at 11 km s^{-1} with respect to the local gas.

Simulations are run using a 3D hydrodynamics code that solves for the equations of hydrodynamics on a Cartesian grid [21]. The gravity of the plan-

etoid is included, where the radius $R = 3000$ km and the mass $M = 0.057 M_{\oplus}$. In this abstract, we present the results for adiabatic simulations with planetoid speeds of 7, 9, and 11 km/s with respect to the gas. The pre-shock gas temperature and density are 300 K and 10^{-9} g/cc, respectively. Gas and particles are coupled as described in [22], with an additional algorithm for handling the stiff drag regime. For the cases presented here, grains are strongly coupled to the gas.

Results: Structural differences between 2D and 3D bow shocks are highly significant (not shown). The standoff distance of the bow shock is about twice as large in the 2D case than in 3D. This increases the chances of grains striking the planetoid. The bow shock also has a shallower opening angle in 3D.

Figures 1-3 show cross sections of 3D shocks for relative speeds of 7, 9, and 11 km/s. Bow and tail shocks form, creating multiple heating locations. There are also narrow, high-temperature spikes that trail the planetoids. These regions are very low density and are largely dust-free. Figures 4-6 show grains that pass completely around the planetoid. Particles correspond to impact parameters between 1500 and 3000 km for the 7 and 9 km/s shocks and 2000-4000 km for the 11 km/s shock. Each profile has a characteristic shape. First, there is a rapid rise in temperature due to the bow shock. This is followed by rapid cooling as the gas passes by the planet and expands. The grains then encounter a tail shock, causing a second, less severe heating, followed again by cooling.

At 7 km/s, the corresponding cooling rate between 1800 and 1400 K (crystallization temperature range) is around 2000 to 3000 K/hr after bow shock passage. All of the followed grains drop below 1400 K before being reheated. The 9 km/s shock shows a more prolonged cooling of about 1000 K/hr. In addition, several grains show trajectories that never drop below 1400 K before reaching the tail shock, which then cools at about 300 K/hr after a second heating episode. Finally, the 11 km/s shock shows an extreme heating event, with post-bow shock cooling rates between 500 and 1500 K/hr. The tail shock is also very strong, with post tail-shock cooling rates around 500 K/hr.

Overall, bow shocks produce complex temperature profiles that are not monotonically decreasing in the post-shock region. A range of solids could be produced by these shocks, although it is unclear what those solids would be. The high cooling rates found here for the 7 and 9 km/s shocks may be conducive to a range of chondrule textures. These simulations form a fiducial for understanding the more complicated cases of radiative shocks, which will be presented during the meeting.

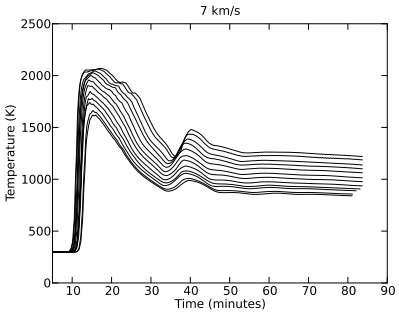

Figure 4: Temperature profiles taken from simulation shown in Figure 1. Cooling is very efficient due to expansion of the gas behind the bow shock. This three-dimensional structure severely limits the length scale over which the post-shock gas will remain hot. However, multiple heating events occur. The hottest trajectory shown dips below 1400 K for about 8 min, and is then reheated above 1400 K for a short duration. The region downwind of the tail shock keeps the gas warm for a protracted period.

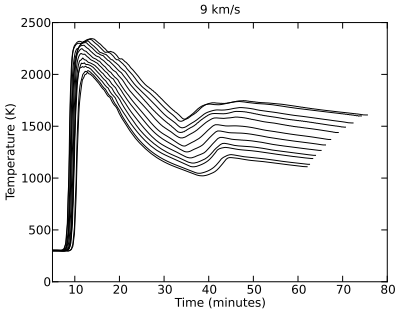

Figure 5: Similar to Figure 4, but for the $9\,\mathrm{km\,s^{-1}}$ shock. The temperature spike resulting from the tail shock becomes much more pronounced. The duration shown in the plot is shorter than in Figure 4 due to the faster relative gas speed.

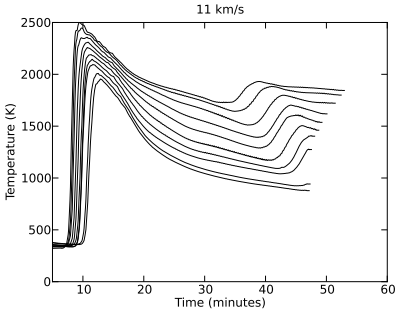

Figure 6: Similar to Figure 5, but for the $11\,\mathrm{km\,s^{-1}}$ shock. The bow and tail shocks in this case keep post-shock temperatures above 1400 K. In this case, grains may stay warm for hours. As in Figure 5, the duration is in this plot is shorter than in Figure 4 due to the faster relative gas speed.

References: [1] Chambers 2001, *Icar*, 152, 205 [2] Matsumura et al. 2010, *ApJ*, 714, 194 [3] Walsh et al., 2011, *Nat*, 475, 206. [4] Hansen 2009, *ApJ*, 703, 1131. [5] Dauphas & Pourmond, 2011, *Nat*, 472, 489. [6] Ciesla et al., 2004, *MAPS* 38, 1809. [7] Morris & Desch *ApJ*, 722, 1474 [8] Morris et al. 2010b, *MAPS*, 73, 5215. [9] Kita, N. T. et. al., 2000. *GCA*, 64, 3913. [10] Mostéfaoui, S. et. al., 2002, *MAPS*, 37,421. [11] Kita et al., 2005, in *Chondrites and the PPD*, 558. [12] Kurahashi, E. et. al., 2008. *GCA*, 72, 3865. [13] Rudraswami, N. G. et. al., 2008, *EPSL*, 274, 93. [14] Villeneuve et al., 2009, *Science*, 325, 985. [15] Desch et al., 2005, *Chondrites and the PPD*, 341, 849. [16] Desch et al., 2010, *ApJ*, 725, 692. [17] Morris et al. 2012, *ApJ*, 752, 27. [18] Hood 1998, *MAPS*, 33, 97. [19] Boley et al. 2007, *ApJ*, 665, 1254 [20] Galvagni et al. 2012, *MNRAS*, 427, 1725 [21] BoxzyHydro is a code written and maintained by A. C. Boley. [22] Boley & Durisen 2010, *ApJ*, 724, 618